

# Shape Matching via Quotient Spaces

Maks Ovsjanikov<sup>#</sup>    Quentin Mérigot<sup>b</sup>    Viorica Pătrăucean<sup>#</sup>    Leonidas Guibas<sup>b</sup>  
<sup>#</sup>LIX, École Polytechnique    <sup>b</sup>LJK, Université Joseph Fourier / CNRS    <sup>b</sup>Stanford University



**Figure 1:** The proposed framework for isometric shape matching allows establishing dense correspondences between symmetric shapes in a principled way. Here, we first estimate a single map in an appropriate quotient space and then use it to generate 8 different point-to-point maps between two octopus models. Each correspondence is shown by transferring the XYZ functions from the target onto the source and rendering them as RGB channels on the mesh. Note, e.g. the location of the orange arm.

## Abstract

We introduce a novel method for non-rigid shape matching, designed to address the symmetric ambiguity problem present when matching shapes with intrinsic symmetries. Unlike the majority of existing methods which try to overcome this ambiguity by sampling a set of landmark correspondences, we address this problem directly by performing shape matching in an appropriate quotient space, where the symmetry has been identified and factored out. This allows us to both simplify the shape matching problem by matching between subspaces, and to return multiple solutions with equally good dense correspondences. Remarkably, both symmetry detection and shape matching are done without establishing any landmark correspondences between either points or parts of the shapes. This allows us to avoid an expensive combinatorial search present in most intrinsic symmetry detection and shape matching methods. We compare our technique with state-of-the-art methods and show that superior performance can be achieved both when the symmetry on each shape is known and when it needs to be estimated.

Categories and Subject Descriptors (according to ACM CCS): I.3.3 [Computer Graphics]: — Shape Analysis.

## 1. Introduction

Shape matching is one of the most fundamental and best-studied problems in digital geometry processing. While rigid shape matching is a relatively well understood, finding correspondences between pairs of shapes undergoing non-rigid deformations, such as articulated motion, remains challenging. Nevertheless, a large number of methods have recently been proposed to address this problem [BBK06, HAWG08, LF09, TBW\*09, OMMG10, KLF11, OBCS\*12, SY13]. Perhaps the most common approach to non-rigid shape matching is to phrase the problem as finding intrinsic near isometries — correspondences that approximately preserve geodesic distances between pairs of points on the

shapes. The space of intrinsic isometries is appealing both because it approximates natural shape deformations based on articulated motion and because it admits low-dimensional parameterizations — under certain conditions it has been shown that fixing a small set of landmark correspondences uniquely determines the dense map between a pair of shapes [LF09, OMMG10].

At the same time, one of the difficulties in applying the isometric shape deformation model in practice is that many organic and man-made shapes exhibit symmetries, which can result in approximate self-isometries. This means, in particular, that when trying to find an intrinsic isometry between a pair of symmetric shapes, such as a pair of humans, there

exist at least two equally good solutions. In the intrinsic setting, many valuable cues for distinguishing these, such as extrinsic orientation, may not be available. Worse still, the presence of approximate symmetries can lead to extreme instabilities during the solution process [OHG11].

The main goal of our paper is to give a theoretical framework and a practical pipeline which lead to an efficient and stable solution for the isometric shape matching problem in the presence of symmetries (Figure 1).

The majority of existing methods try to address this problem by fixing landmark correspondences either between points [LF09, OMMG10] or between parts of shapes [OBCS\*12], to “break” the ambiguity in matching symmetric shapes. However, this does not circumvent the underlying problem, since reliably establishing the landmark correspondences can in itself be challenging and error-prone, particularly because of the symmetric ambiguity in the selection. Purely intrinsic methods are typically able to return an approximation of only one of the multiple possible correspondences, without any indication that another equally good solution is present. For this reason, common shape matching benchmarks, (e.g. [KLF11]), consider as correct either of the two correspondences.

Rather than trying to ignore the symmetric ambiguity problem or bypass it by fixing landmark correspondences, we propose to take advantage of it, by incorporating the symmetry information directly into the matching formulation. This idea is in line with several works that stress the great discriminative potential of symmetry cues as features for object recognition or categorization [PLC\*08]. Indeed, one of our observations is that the presence of a symmetry should make shape matching *easier*, since intuitively only halves of the shapes need to be matched. Thus, we propose to perform shape matching in a reduced (quotient) space in which the symmetric parts have been identified and the distinction between them factored out. Carrying out this identification literally on the level of points on the shape, however, is problematic, as the symmetrized object is not itself naturally represented as a manifold or a mesh.

At the heart of our method is the dual functional map representation introduced in [OBCS\*12]. In that work, the authors pointed out that while the set of points on a curved surface can be very complex, the set of square integrable functions defined on the surface forms a vector space, and isometric shape matching can be phrased as finding a linear map between a pair of vector spaces. In our work, we exploit this vector space structure to define an appropriate *quotient space* of the functional space, which efficiently incorporates the symmetry information of the shapes to reduce the complexity of the shape matching problem. This is due to the fact that the linear-algebraic vector space structure of the functional space allows operations such as subspace identification and projection to be handled in a natural, seamless and efficient way.

As input to our method, we assume that we are given a pair of approximately isometric shapes without correspondences, but with a known symmetry map on one of the shapes. Our goal is to use this information to a) detect the symmetry on the second shape, and b) obtain both direct and symmetric dense correspondences between the pair of shapes. Remarkably, our method achieves high quality correspondences without requiring any landmark point or part correspondences in the matching process. This is in sharp contrast to existing shape matching methods which uniformly rely on some notion of landmark correspondences. Finally, while we focus on reflectional symmetries in this paper, our framework can handle other types of symmetry, although extracting the final dense map in the general case is not straightforward and constitutes a direction of future research.

### 1.1. Related work

Although shape matching is an extremely well-studied problem, there are relatively few methods that try to study and systematically address the symmetric ambiguity present in isometric shape matching.

A number of methods have tried to consider this problem from the point of view of optimal placement of landmark correspondences. In the context of rigid matching, Gelfand et al. [GIRL03] proposed a landmark placement method, designed to alleviate the slippage problem, present when matching two approximately slippable surfaces.

In non-rigid shape matching, Ovsjanikov et al. [OHG11] pointed out that stability of isometric shape matching is intimately related to the symmetry structure of the shapes, and proposed an efficient landmark selection procedure, designed to improve shape matching performance in practice. Tevs and colleagues [TBW\*11] proposed a guided landmark selection process for shape matching, which adds landmark points according to the amount of information contained in them, as measured by the entropy of an appropriate probability distribution. In [SY13], the authors used a combinatorial multi-resolution matching approach, which tracks several possible correspondence maps at the first (coarser) levels, and the one that minimizes the geodesic distortion is kept at the finer sampling levels. Although diminished, symmetric flipping is still present in the final map.

Conceptually, our method is similar to classic sub-string matching techniques [KMP77, BM77], where the self-similarity of the pattern string is first taken into account before the matching, and then used to simplify and speed up the matching process into the text string.

In the same spirit, recent works in shape analysis try to explicitly use the symmetry information in order to lighten up essential tasks like shape matching [LKF12], shape segmentation [LCDF10], or symmetry classification [RBBK10]. Specifically, Liu et al. [LKF12] reduce the shape matching problem to a symmetry axis alignment problem. First

they use a combinatorial approach to extract the symmetry axes on both shapes, which are then aligned using a 1D string matching algorithm. Eventually, a dense correspondence map between the shapes is obtained by extrapolating the correspondences found on the symmetry axes. Although the method exhibits good performance on intrinsically symmetric shapes, the use of this approach is limited to shapes where reliable 1D symmetry axes can be extracted.

In [LCDF10], the authors propose a symmetry-factored embedding and distance, according to which symmetric points on a shape get mapped to the same point in the new embedding. This proves to be useful in applications like symmetry orbit approximation or segmentation of symmetric shapes. Our approach is directly inspired by this work and extends it to finding correspondences between *pairs* of shapes by using the symmetry invariant function space described in [LCDF10] for shape matching.

In [RBBK10], Raviv et al. analyze and explore the group of symmetries defined on a shape. In a *bottom-up* manner, they use point landmarks to identify *symmetry generators*, which are then composed to recover the complete symmetry group. While elegantly handling different types of symmetry, this approach is parameter-dependent and can lead to an incomplete symmetry group, if one of the symmetry generators is not properly identified.

Our approach is fundamentally different from the aforementioned works in that the goal is to first recover symmetries as consistent dense maps, and then use this information to find multiple equally good dense correspondences between shapes without any landmark correspondences. Performing shape matching using symmetry information removes the symmetry flipping problem.

**Outline:** In Section 2 we briefly recall the functional map framework. Section 3 shows how this framework can be used to *decompose* maps into parts which can be estimated independently. In Section 4 we use this observation to introduce the *quotient space matching* method, which allows us to compute a dense correspondence between shapes with a known symmetry structure. We then extend this approach to *semi-quotient matching* (Section 5), which is applicable in case the symmetry is known on only one of the shapes. Section 6 describes in detail the application of the proposed framework for the particular case of reflectional shapes, and Section 7 presents the results obtained using our techniques.

## 2. Functional Maps

In order to describe our approach, we first give an overview of the functional map framework introduced in [OBCS\*12].

**Notation.** We call *shape* a compact smooth surface  $M$ . The intrinsic distance between points on  $M$  is denoted by  $d_M$  and the Laplace-Beltrami operator by  $\Delta_M$ . As is common, we

denote  $L^2(M)$  the space of square-integrable functions on  $M$ . This space is endowed with the scalar product  $\langle \cdot, \cdot \rangle$  and Hilbert norm  $\|\cdot\|$ .  $\text{Id}_M$  denotes the identity map of  $M$ .

**Functional map framework.** Given a pair of shapes  $M$  and  $N$ , a *functional map* between  $M$  and  $N$  is a bounded linear map  $\mathcal{T}$  between the vector spaces  $L^2(M)$  and  $L^2(N)$ . For instance, one can associate to every continuous map  $T : N \rightarrow M$  a functional map from the space  $L^2(M)$  to  $L^2(N)$  using the formula  $\mathcal{T}(f) := f \circ T$ .

Given two orthonormal bases  $(\phi_i^M)$  and  $(\phi_i^N)$  of the spaces  $L^2(M)$  and  $L^2(N)$ , such a linear map  $\mathcal{T}$  can be represented by an infinite matrix  $C$ , defined by  $C_{ij} = \langle \mathcal{T}(\phi_j^M), \phi_i^N \rangle$ . The authors of [OBCS\*12] pointed out that by using a multi-scale basis, such as the one consisting of the eigenfunctions of  $\Delta_M$  and  $\Delta_N$ , the map  $\mathcal{T}$  can be well-approximated by finite matrices  $C_n := (C_{ij})_{1 \leq i, j \leq n}$  for a fixed  $n$ . Moreover, one can recover  $C_n$  in practice by formulating constraints of the type  $C_n f = g$ , where  $f$  and  $g$  are corresponding functions on  $M$  and  $N$  respectively. Note that  $n$  linearly independent constraints of this type uniquely define the matrix  $C_n$ .

The functional correspondence constraints used in [OBCS\*12] are of two types. The functions  $f$  and  $g$  can be local shape *descriptors*, i.e. functions derived from the geometry of the shapes. Common robust descriptors include the heat kernel signature (HKS) [SOG09] at a particular time  $t$  or the Wave Kernel Signature (WKS) [ASC11] for a logarithmic energy parameter  $c$ . In practice, these constraints are usually not sufficient for obtaining a matrix representing a point-to-point map, as they do not resolve symmetric ambiguities. One therefore needs to add segment preservation constraints, i.e.  $C_n f = g$  where  $f$  and  $g$  are indicator functions of the same segment on the two shapes. Establishing part preservation constraints, however, is computationally expensive and error-prone. Our goal here is to derive a shape matching procedure that does not require any landmark correspondence on the level of parts or points.

Whilst in [OBCS\*12], the authors highlighted the fact that the functional map representation naturally supports certain algebraic operations such as map sum, difference and composition, in this paper we explore the so-called functional map *decomposition*, which allows us to split the functional map between two shapes into parts, each of which can be estimated independently. This map decomposition corresponds to the decomposition of the vector spaces of functions on the two shapes into linear subspaces. In this work we consider the particular decomposition of a vector space into its symmetric and anti-symmetric subspaces, as it allows us to address the ambiguity present when matching shapes with intrinsic symmetries.

## 3. Decomposition of Functional Isometries

Recall that an *isometry* between two shapes is a map that preserves distances between points. Throughout this paper

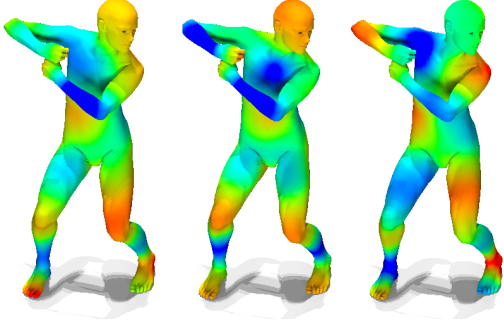


**Figure 2:** A function defined on a shape  $M$  (left), and its projection onto the space of symmetric functions  $L_+^2(M)$  (center) and anti-symmetric functions  $L_-^2(M)$  (right).

we also assume that a *symmetry* is an isometry between a shape and itself. A *functional isometry* is a functional map  $\mathcal{T}$  such that  $\|\mathcal{T}f\| = \|f\|$  for every function  $f$  on the source shape. Note that a functional map induced by an isometry is a functional isometry, but the converse is not true in general.

**Space of symmetric functions  $L_+^2(M)$ .** We recall some results on the space of symmetric functions on a shape, some of which have also been used in [LCDF10]. Note however that Lemmas 3.1 and 3.2 are specific to the functional map framework.

Let  $\text{Sym}(M)$  be the group of symmetries of a shape  $M$ . The subspace of  $L^2(M)$  consisting of functions that are invariant to symmetry is

$$L_+^2(M) = \{f \in L^2(M); \forall S \in \text{Sym}(M), f \circ S = f\}.$$

When the number of symmetries is finite, the space  $L_+^2(M)$  agrees with the space  $L^2(\bar{M})$ , where  $\bar{M}$  is the quotient of  $M$  by its symmetry group. In this paper, we show how the space of symmetric functions can be used in practice to perform computations that involve the quotient shape, but without actually computing this quotient.

The orthogonal complement of the subspace  $L_+^2(M)$  is denoted  $L_-^2(M)$ , and the orthogonal projections on these two spaces are denoted  $\pi_{\pm}$ . When the symmetry group has cardinality  $k$ , these orthogonal projections are given as:

$$\pi_+(f) = \frac{1}{k} \sum_{S \in \text{Sym}(M)} f \circ S, \quad \pi_- = \text{Id}_M - \pi_+. \quad (1)$$

Figure 2 shows an example of a shape and a function  $f$ , projected onto the space  $L_+^2(M)$  and  $L_-^2(M)$ .

**Symmetric eigenvectors of  $\Delta_M$ .** The Laplace-Beltrami operator  $\Delta_M$  has the well-known property of commuting with isometries. This means that if  $T: N \rightarrow M$  is an isometry, then for any smooth function  $f$  in  $L^2(M)$ ,

$$(\Delta_M f) \circ T = \Delta_N(f \circ T). \quad (2)$$

Using Eq. (1), this property implies in particular that  $\Delta_M$

maps the space of symmetric functions  $L_+^2(M)$  to itself. We consider a basis of the space  $L^2(M)$  consisting of eigenfunctions of the Laplace-Beltrami operator, that is  $(v^i)_{i \geq 0}$  such that  $\Delta_M v^i = \lambda_i v^i$ . We assume that the eigenvalues are sorted in increasing order.

**Lemma 3.1** There exists an orthogonal basis of the space of symmetric functions  $L_+^2(M)$  consisting only of eigenvectors of the Laplace-Beltrami operator, i.e.  $\Delta_M v_+^i = \lambda_i v_+^i$ .

*Proof* Consider an eigenpair  $(\lambda_i, v^i)$  of  $\Delta_M$ . By the commutativity property (2), one has

$$\Delta_M(v_i \circ S) = (\Delta_M v^i) \circ S = \lambda_i v^i \circ S$$

for any symmetry  $S$  of  $M$ . Summing these equalities over all symmetries  $S$  in the group  $\text{Sym}(M)$ , and using (1), this implies that  $\pi_+ v^i$  is an eigenvector of the Laplace-Beltrami operator. Since  $L_+^2(M) = \pi_+(L^2(M))$ , we can extract from these vectors a basis of  $L_+^2(M)$ .  $\square$

**Functional map decomposition.** Equation (1) implies that any functional isometry  $\mathcal{T}$  between two shapes  $M$  and  $N$  can be partitioned into two parts  $\mathcal{T}_{\pm}$  that act respectively on the space of symmetric functions and on its orthogonal complement. Precisely,

$$\mathcal{T}_{\pm} : L_{\pm}^2(M) \rightarrow L_{\pm}^2(N), \quad \mathcal{T}_{\pm}(f) = \pi_{\pm} \circ \mathcal{T}(f). \quad (3)$$

Moreover, these two maps  $\mathcal{T}_{\pm}$  are functional isometries between their source and target spaces.

The following lemma, which is at the heart of our approach, shows that although there may be multiple functional maps corresponding to isometries between two shapes, the symmetric parts of these maps coincide.

**Lemma 3.2** Given two isometric shapes  $M$  and  $N$ , consider the two functional maps  $\mathcal{T}, \mathcal{S}$  induced by two different isometries  $T, S: N \rightarrow M$ , then  $\mathcal{T}_+ = \mathcal{S}_+$ .

*Proof* By assumption,  $T \circ S^{-1}$  is a symmetry of  $M$  and for any symmetric function  $f$  on  $M$  one has  $f \circ T \circ S^{-1} = f$ . Thus,  $f \circ T = f \circ S$  for all symmetric  $f$ , i.e.  $\mathcal{T}_+ = \mathcal{S}_+$ .  $\square$

#### 4. Quotient-Space Matching

In the functional map framework, one is searching for a functional map  $\mathcal{T}^*$  that is induced by an isometry from  $N$  to  $M$ . One of our main observations is that the symmetric part  $\mathcal{T}_+^*$  of the unknown map  $\mathcal{T}^*$  is significantly easier to compute than the anti-symmetric part, for the following two reasons:

- When the shapes  $M$  and  $N$  have non-trivial symmetry groups, there exist multiple different isometries between  $N$  and  $M$ , which induce different functional maps between the spaces  $L^2(M)$  and  $L^2(N)$ , while, as shown in Lemma 3.2, their symmetric parts  $\mathcal{T}_+^*$  coincide.
- Intrinsic descriptors, such as the HKS or WKS, are symmetric functions on the shape, and do not give any infor-

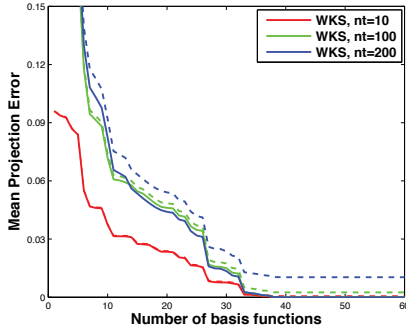


**Figure 3:** Average quadratic error obtained when projecting the descriptors on the space  $E_k$  spanned by the first  $k$  eigenfunctions of the Laplace-Beltrami operator (solid lines) and the symmetric part of this space only (dashed lines).

mation on the anti-symmetric part of the optimal map. In other words, there are as many linearly independent function preservation constraints for the symmetric part  $\mathcal{T}_+$  as for the full functional map  $\mathcal{T}$  even though the domain and range spaces of the former are smaller (see Figure 3).

In this section, we show how to exploit these remarks in a pipeline that is adapted from [OBBS\*12] in order to compute functional maps  $\mathcal{T}_+$  from symmetric functions to symmetric functions. Since computing the functional map boils down to a linear solve, we first discuss rank-deficiency issues and ways to increase the rank of the linear system, and then we introduce the full algorithm for quotient-space matching.

#### 4.1. Rank of the descriptors.

Consider the finite space  $E_k(M)$  spanned by the  $k$  eigenfunctions of the Laplace-Beltrami operator with  $k$  smallest eigenvalues, and  $E_{\pm}^k(M) := \pi_{\pm}(M)$  the symmetric and anti-symmetric parts of this space. A natural question is how to construct a family of descriptors that span the whole space  $E_{\pm}^k(M)$ . More realistically, we would like to maximize the rank of the linear space spanned by the chosen signatures. Figure 4 (solid lines) shows the rank of the space spanned by Wave Kernel Signatures [ASC11] taken at certain energy levels  $(c_i)_{1 \leq i \leq \ell}$ , as a function of the number of energy levels. We note that beyond a certain point adding more energy levels does not help to increase the rank of the system.

**Increasing the rank.** The rank of the descriptor space can be increased by producing derived descriptors indicating where certain values of the original descriptors occur on the shape. This can be done using a very simple partitioning technique. We split every descriptor  $f$  from  $M$  to an interval  $[a_f, b_f]$  into a finite number of derived descriptors  $f_1, \dots, f_s$  defined by the formula

$$f_i(x) := \exp\left(-\frac{(f(x) - a_{f,i})^2}{\sigma_f^2}\right),$$

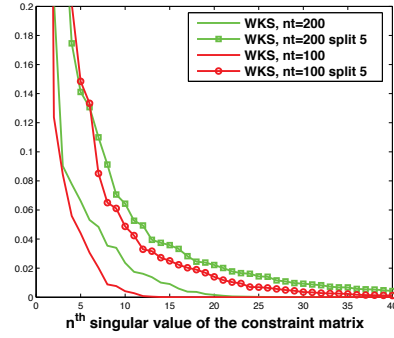


**Figure 4:** Singular values of the descriptors constraint matrix before and after the splitting. Note that increasing the number of levels does not help to increase the rank beyond a certain point, even after the splitting; hence regularization is also required.

where  $\sigma_f = (b_f - a_f)/s$  and  $a_{f,i} = a_f + i\sigma_f$ . We apply the same transformation to the corresponding descriptors  $g$  on the second shape  $N$ . We then replace the descriptor preservation constraint  $\mathcal{T}f = g$  by  $s$  such derived constraints  $\mathcal{T}f_i = g_i$ . Intuitively, this splitting operation re-enforces the local information contained in the original descriptors, augmenting the rank of the matrix of descriptors (see Figure 4, marker lines), which improves the estimated functional map.

#### 4.2. Regularization

Even with splitting, the descriptors usually do not span the whole space of symmetric functions. This means that the signature preservation constraints are not sufficient to define the unknown map  $\mathcal{T}_+^*$  uniquely, and one needs to add regularization terms in the optimization in order to converge to a good approximation of  $\mathcal{T}_+^*$ . The following Lemma lists a few properties of the optimal map  $\mathcal{T}_+^*$  that follows from §3. As in [OBBS\*12], these properties are used as regularizations in the map estimation algorithm.

We denote by  $\delta^{x,t}$  the distribution of heat obtained by applying the heat flow from a Dirac mass at  $x$  for a time  $t$ . The symmetrization of this function is denoted  $\delta_+^{x,t}$ .

**Lemma 4.1** The map  $\mathcal{T}_+^*$  satisfies the following properties:

- (i) Commutativity with the Laplace-Beltrami operator, i.e.  $\Delta_N(\mathcal{T}_+^*f) = \mathcal{T}_+^*(\Delta_M f)$  for every function  $f$  in  $L_+^2(M)$ .
- (ii)  $\mathcal{T}_+^*$  is an isometry from  $L_+^2(M)$  to  $L_+^2(N)$ .
- (iii) For every point  $x$  on  $M$ , there exists a point  $y$  in  $N$  such that for all times  $t > 0$  one has  $\mathcal{T}_+^* \delta_+^{x,t} = \delta_+^{y,t}$ .

These properties follow directly from the fact that  $\pi_+$  commutes with the Laplace-Beltrami operator, from Lemma 3.1, and from Eq. (3).

---

**Algorithm 1:** Quotient-space shape matching

---

**Input:** Shapes  $M, N$ , represented as triangle meshes, symmetries  $S_M : M \rightarrow M, S_N : N \rightarrow N$

**Output:** Point to orbit map  $M \rightarrow N/S_N$ . Dense maps  $M \rightarrow N$  in case of reflectional symmetries.

- 1 Compute a multiscale basis  $(v_+^i)$  and  $(w_+^i)$  for  $L_+^2(M), L_+^2(N)$ , by extracting a multiscale basis for  $L^2(M), L^2(N)$  and restricting to functions, invariant to  $S_M$  and  $S_N$  respectively.
  - 2 Compute a set of descriptors  $(f_i), (g_i)$  on  $M$  and  $N$  (e.g. WKS for a particular energy level  $c_i$ ), and represent them as vectors of coefficients in  $(v_+^i)$  and  $(w_+^i)$ .
  - 3 Formulate commutativity constraints  $C\Delta_M^+ = \Delta_N^+C$ , where  $\Delta_M^+$  is the projection of  $\Delta_M$  onto  $(v_+^i)$ .
  - 4 Estimate the initial  $C_0$  using a least squares system.
  - 5 Refine  $C_0$  using quotient-ICP, and convert it to a point-to-orbit map. In case of reflectional symmetries, convert to a point-to-point map.
- 

### 4.3. Algorithm

Our quotient-space matching algorithm follows the pipeline proposed in [OBCS\*12]. The main difference is that we are searching for a functional map between the spaces of symmetric functions  $L_+^2(M)$  to  $L_+^2(N)$ . The main steps of the algorithm are summarized in Algorithm 1.

The quotient matching algorithm tries to approximate the unknown functional map  $\mathcal{T}_+^*$  by a matrix  $(C_{ij})$  in these multi-resolution bases. These bases are obtained by symmetrizing Laplace-Beltrami eigenvectors using the operator  $\pi_+$  and by pruning the redundant vectors. The basis of the space  $L_+^2(M)$  constructed this way is denoted  $(v_+^i)$ , with corresponding eigenvalues  $\lambda_i$ . On  $L_+^2(N)$ , they are denoted respectively  $(w_+^j)$  and  $\mu_j$ . In a first step, we construct an initial estimation  $C_0$  of the optimal map by enforcing in a least-square sense signature preservation and Laplace-Beltrami commutativity. This map is then refined using a variant of the *iterative closest point algorithm* called quotient-ICP. More details about the implementation of both steps of the algorithm can be found in §6 of [OBCS\*12].

**Initial estimation.** The initial matrix  $C_0$  is constructed by minimizing the functional  $E_0(C) := E_{\text{sig}}(C) + E_{\text{com}}(C)$ . The first term  $E_{\text{sig}}$  corresponds to the signature preservation defect, and the second term  $E_{\text{com}}$  corresponds to the defect of commutativity with the Laplace-Beltrami operator, as justified by Lemma 4.1(i). These defects are measured in a least-square sense:

$$E_{\text{com}}(C) = \sum_{i,j} C_{ij}^2 (\lambda_i - \mu_j)^2, \quad E_{\text{sig}}(C) = \sum_s \|C_{ij} f_s - g_s\|^2.$$

The functions  $(f_s)$  and  $(g_s)$  are corresponding symmetric signatures on  $M$  and  $N$ . In our experiments, we used WKS functions as signatures, similar to the [OBCS\*12] setting.

**Quotient-ICP.** The matrix  $C_i$  is then refined iteratively using a variant of the ICP algorithm, which is motivated by Lemma 4.1 (ii) and (iii). We first construct a sparse sampling

$S$  of  $M$ ; then at every step  $i$ , we compute the map

$$T_i : x \in S \mapsto \arg \min_{y \in N} \left\| \delta_+^{y,t} - C_i \delta_+^{x,t} \right\|.$$

This nearest-neighbor computation can be easily performed using an adapted data structure such as a  $k$ -d-tree. The updated matrix  $C_{i+1}$  is then obtained by computing the singular value decomposition of the matrix  $\sum_{x \in S} \delta_+^{T_i(x),t} (\delta_+^{x,t})^T$ , after replacing all of its singular values by one.

### 4.4. Conversion to point-to-orbit and point-to-point.

The map  $\mathcal{T}_+$  obtained as an output of the algorithm presented above can be converted to a point-to-orbit map, where every point  $x$  in  $M$  is mapped to a set of the form  $\mathcal{O}_y := \{S(y); S \in \text{Sym}(N)\}$ . This conversion is performed using the algorithm used in [OBCS\*12] to compute the point-to-point map: given a query point  $x$  in  $M$ , one computes a point  $T(x)$  that minimizes

$$\arg \min_{y \in N} \left\| \mathcal{T}_+ \delta_+^{x,t} - \delta_+^{y,t} \right\|.$$

Note that one should not expect the point-to-point map  $T$  to be continuous, as the choice between a point  $y$  in  $N$  and a symmetric point  $y'$  is completely arbitrary. As shown in Section 7.1 the map  $R : x \mapsto \mathcal{O}_{T(x)}$  from points on the first shape  $M$  to *orbits* on the second shape  $N$  turns out to be continuous in most practical cases.

**Point-to-point maps.** A *fundamental domain* of  $M$  is a closed set  $D \subseteq M$  such that for every symmetry  $S$  of  $M$  the restriction of  $S$  to the interior of  $D$  is one-to-one. Moreover, we require that the family of sets  $S(D)$  cover  $M$ . We call decomposition of  $M$  into fundamental domains a covering  $(D_i)_{1 \leq i \leq n}$  of  $M$  by images of  $D$  under symmetries, such that the sets  $(D_i)$  have pairwise disjoint interior. Now assume that we are given consistent decompositions  $(D_i)_{1 \leq i \leq n}$  and  $(E_i)_{1 \leq i \leq n}$  of the shapes  $M$  and  $N$  into fundamental domains. Note that such a consistent decomposition can be found when both shapes  $M$  and  $N$  have a single reflectional symmetry, as shown in Section 6. In this setting, it is possible to convert a point-to-orbit map  $R$  into a consistent point-to-point map  $\bar{T}$ , by defining the image of a point  $x$  that belongs to a fundamental domain  $D_i \subseteq M$  as the unique point in the intersection of the orbit  $\mathcal{O}_{T(x)}$  with the corresponding fundamental domain  $E_i$ .

### 5. Semi-Quotient Matching

A more realistic scenario when matching two symmetric shapes is that the symmetry, or rather the space of symmetric functions  $L_+$ , is known for only one of the two shapes under consideration. This is the case for instance when matching two poses of a shape, one of which possesses an ambient reflectional symmetry — such as the rest pose of a human shape. In this section we show how our approach can be used to *transfer* the known symmetry information from the target

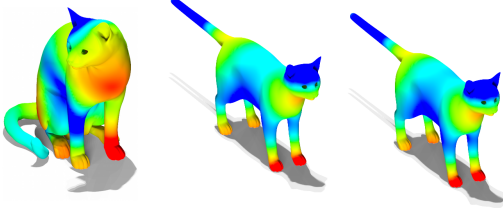


**Figure 5:** For semi-quotient matching we aim to estimate the functional map  $\mathcal{R}^* = \pi_+ \circ \mathcal{T}$  from  $L^2(M)$  to  $L^2_+(N)$ , where only a symmetry on  $N$  is known. Thus, for any function  $f$  on  $M$  (left),  $\mathcal{R}^* f$  is a symmetric function on  $N$ . (center)  $\mathcal{R}^* f$  computed using the ground truth map, and (right) estimated using our method. Note that all isometries  $N \rightarrow M$  induce the same  $\mathcal{R}^*$  making it easier to compute.

shape to the source, and then use the ideas of the previous section to establish the dense correspondence map between the two shapes. Hence, throughout this section, we assume that the source and target shapes  $M$  and  $N$  are isometric, and that we know the space  $L^2_+(N)$  for the target shape *only*.

Let  $T$  be an isometry between  $N$  and  $M$ , and  $\mathcal{T}_\pm^*$  be the decomposition of the functional map  $\mathcal{T}$  induced by  $T$  on the spaces of symmetric and anti-symmetric functions. The goal is to recover the functional map  $\mathcal{R}^*$  from  $L^2(M)$  to  $L^2_+(N)$ , which maps a function in  $M$  to the symmetrization of the corresponding function on  $N$ . This means that  $\mathcal{R}^* = \pi_+ \circ \mathcal{T}$ , where  $\pi_+$  is the projection onto the space of symmetric functions on  $N$  (see Fig. 5). Note that Lemma 3.2 also holds in this case, which means that the optimal map is uniquely defined, making it easier to estimate in practice. In this scenario, however, the map  $\mathcal{R}^*$  cannot be expected to be an isometry, as the dimension of its domain and range spaces are different. The following Lemma shows that the regularization induced by LB commutativity and quotient-ICP can be adapted with minor modifications of the algorithm.

**Lemma 5.1** The map  $\mathcal{R}^*$  satisfies the following properties:

- (i) Commutativity with the Laplace-Beltrami operator, i.e.  $\Delta_N(\mathcal{R}^* f) = \mathcal{R}^*(\Delta_M f)$  for every function  $f$  in  $L^2(M)$ .
- (ii) The orthogonal complement of  $\text{Ker } \mathcal{R}^*$  is  $L^2_+(M)$ .
- (iii) The restriction of  $\mathcal{R}^*$  to  $L^2_+(M)$  is an isometry.
- (iv) For every point  $x$  on  $M$ , there exists a point  $y$  in  $N$  such that for all times  $t > 0$  one has  $\mathcal{R}^* \delta^{x,t} = \delta^{y,t}$ .

The algorithm for semi-quotient matching is then very similar to the one presented in Section 5. The main difference is in the semi-quotient ICP step, which we describe below.

**Semi-quotient ICP.** For semi-quotient matching, the matrix  $C_i$  that we compute has dimension

$$\dim(E^k(M)) \times \dim(E_+^k(N)) \simeq k \times (k/2).$$

Properties (ii) and (iii) of Lemma 5.1 suggest to estimate first  $L^2_+(M)$  as the orthogonal complement of the kernel, and then

to enforce the isometry property on the subspace  $L^2_+(M)$ . Using the same notations as in the previous section, the ICP projection step can be modified as follows. First, compute

$$T_i(x) := \arg \min_{y \in Y} \left\| \delta_+^{y,t} - C \delta^{x,t} \right\|.$$

Then, compute the singular value decomposition of the *rectangular* covariance matrix  $M_i = \sum_{x \in S} \delta_+^{T_i(x),t} (\delta^{x,t})^T$ . The refined matrix  $C_{i+1}$  is then obtained by replacing all the singular values of  $M_i$  by one.

**Function transfer from  $L^2_+(N)$  to  $L^2(M)$ .** The pseudo-inverse of the functional map  $\mathcal{R} : L^2(M) \rightarrow L^2_+(N)$  can be used to transfer symmetric functions from the second shape to the first shape. In practice, however, we observe that the space spanned by the first few eigenvectors of the Laplace-Beltrami operator does not allow us to approximate well certain functions. In order to be able to transfer any symmetric function defined on  $N$ , we convert the map  $\mathcal{R}$  into a point-to-orbit map  $R$  using the same algorithm as in Section 4. The pull-back of a symmetric function  $g$  in  $L^2_+(N)$  is the function  $f$  on  $M$  defined by the formula  $f(x) := g(R(x))$ .

## 6. The Case of Reflectional Symmetries

In this section, we assume that both shapes  $M$  and  $N$  have a single reflectional symmetry. Moreover, we assume that we are given the unique non-trivial symmetry  $S_N$  of the target shape, or that we can estimate it easily. We show how to exploit the information contained in the semi-quotient matching of the previous section in order to pull back the symmetry map from the target shape  $N$  to the source shape  $M$ . Finally, we explain how to construct dense point-to-point matchings between the shapes  $M$  and  $N$ .

A shape has a single reflectional symmetry if its symmetry group contains exactly two symmetries: the identity map  $\text{Id}_M$  and an involutive symmetry  $S_M$ , i.e. such that  $S_M \circ S_M$  is the identity map. Moreover, we assume that the symmetry axis  $M_0 := \{x \in M; S_M(x) = x\}$  separates the shape into two parts, denoted  $M_\ell$  and  $M_r$ , for left and right.

### 6.1. Symmetry transfer

The simplest idea for transferring the symmetry operator from the second shape to the first shape would be to use Eq. (1). When the shape has only two symmetries, this equation implies  $S_M(f) = 2\pi_+(f) - \text{Id}_{L^2(M)}$ , and one could expect to be able to estimate the functional  $S_M$  using the orthogonal projection onto the space of symmetric functions. While elegant in theory, we observe that this idea does not always provide good results in practice.

**Left-right map.** We call *left-right map* of  $M$  the map  $\varepsilon_M$  that maps every point on the left part  $M_\ell$  to  $-1$  and every point on the right part  $M_r$  to  $1$ . The knowledge of the left-right map is equivalent to the knowledge of the left and right parts of  $M$ . Although we do not use this in practice, we also

note that the decomposition of  $M$  into the right and left parts can in principle be recovered from a *single* correspondence between a point  $p_\ell$  and its correspondence  $p_r = S_M(p_\ell)$ , if  $p_\ell \neq p_r$ , by simply considering the intrinsic Voronoi cells of these two points.

Our goal is to use the result of the semi-quotient matching between shapes  $M$  and  $N$  to estimate the left-right map on shape  $M$ . The algorithm from the previous section gives us a map  $\mathcal{R} : L^2(M) \rightarrow L^2_+(N)$ , which can be used to pull back symmetric functions from the target shape  $N$  to  $M$ . Note that this does not allow us to pull back the left-right map of  $N$  directly since this map is anti-symmetric. We can circumvent this difficulty using the following pipeline:

1. Compute the (symmetric) function  $\phi : N \rightarrow \mathbb{R}$  that maps every point  $x$  on  $N$  to the intrinsic distance between  $x$  and the symmetric point  $S_N(x)$ . If speed is important and if the shape  $N$  has an extrinsic reflectional symmetry, one can use the extrinsic distance between  $x$  and  $S_N(x)$ .
2. Pull the function  $\phi$  back on  $M$  as explained in the previous section, thus constructing an approximation  $\tilde{\psi}$  of the function  $\psi : x \in M \mapsto d_M(x, S_M(x))$ .
3. Extract the left and right part of  $M$  using the persistence-based clustering algorithm introduced in [CGOS11]. In this setting, we use the mesh itself as the nearest neighbor graph, and choose the persistence threshold parameter automatically from the persistence diagram so as to yield exactly two clusters  $\tilde{M}_\ell$  and  $\tilde{M}_r$ .

This partition of the shape  $M$  is finally converted to a left-right map  $\tilde{\epsilon}_M$ .

**Symmetry reconstruction.** The approximation  $\tilde{\epsilon}_M$  of the left-right map on  $M$  can then be used to create new descriptors. This means that in addition to the usual descriptor-preservation constraints ( $f_s$ ) that lie in the space of symmetric functions  $L^2_+(M)$ , we can construct anti-symmetric descriptors ( $\pm \tilde{\epsilon}_M f_s$ ). This allows us to use the functional map pipeline from [OBCS\*12] to estimate the symmetry  $S_M$  between  $M$  and itself. We search for a functional map  $\mathcal{S}$  from  $M$  to itself which satisfies the descriptor-preservation constraints  $\mathcal{S} \tilde{\epsilon}_M f_s = -\tilde{\epsilon}_M f_s$  in addition to the standard constraints  $\mathcal{S} f_s = f_s$ . This map is refined using the ICP regularization, and can then be converted to a point-to-point map. The results of this algorithm are reported in Section 7.2.

## 6.2. Pipeline for quotient-based shape matching

One can combine the algorithms of the previous sections in order to construct pairwise matchings between shapes ( $M_i$ ) that are isometric deformations of a shape  $M_1$  with a single reflectional symmetry, which we assume to be known.

1. For every shape  $M_i$ , estimate the left-right map  $\epsilon_{M_i}$  and the space of symmetric functions  $L^2_+(M_i)$  by using the semi-quotient matching and symmetry transfer between  $M_i$  and  $M_1$ , as explained in Section 6.1.

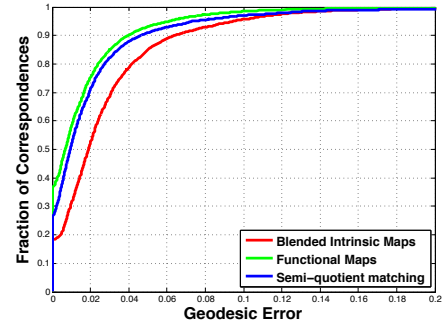


**Figure 6:** Geodesic error for correspondences computed for each shape in the TOSCA dataset to the undeformed shape in the same class, where both the point and its symmetric image are considered as correct.

2. For every pair of shapes we perform quotient-space matching as described in Section 4. This gives us functional maps  $\mathcal{T}_+^{ij} : L_+(M_i) \rightarrow L_+(M_j)$ .

Note that in general, the result of quotient-space matching can only be converted to a point-to-orbit map. However, in the case of reflectional symmetries, we have a consistent decomposition of all shapes into fundamental domains, namely the right part and the left part of the shape.

3. Convert the point-to-orbit map to a consistent point-to-point map by enforcing the preservation of the left and right parts of the shapes as in Section 4.4. We get a second consistent matching by switching the left and right parts. Section 7.3 describes this step in detail.

## 7. Results

The quantitative experimental results given in this section were obtained using the TOSCA dataset, which contains 9 classes of shapes (3 humans, 5 animals, and 1 centaur), 81 shapes in total [KLF11, BBK08]. All shapes exhibit a reflectional symmetry. Each class contains one undeformed version of the shape, except for the class “gorilla”. It is worth mentioning that we first updated the ground truth from the benchmark (with the authors’ permission), in order to obtain a more accurate evaluation, since we observed that some of the landmark correspondences were noisy. We improved the benchmark both by increasing the number and the quality of symmetric correspondences to 50 uniformly distributed pairs of points in each shape class. This ground truth is used for evaluating symmetry detection, and shape matching, when symmetric flipping is allowed.

Following the pipeline given in Section 6.2, we will first report the results of the semi-quotient shape matching method described in Section 5, when matching each shape to the undeformed shape in the same class. In this case, the reflectional symmetry on the undeformed shape is a global extrinsic reflectional symmetry and can therefore be computed easily. Note that we excluded the class “gorilla” from all of

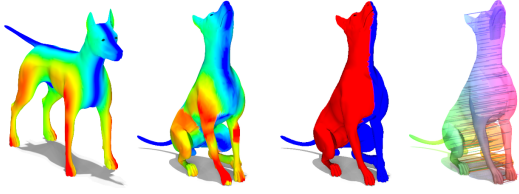


**Figure 7:** The distance function  $d(x, S(x))$  computed on the undeformed shape, the transferred function using the estimated map, result of persistence-based clustering and the final estimated symmetry.

the following examples, because no undeformed version of it is provided. Using the symmetry transfer described in Section 6.1, we get the symmetry map for each shape in the dataset; the quality of these maps is evaluated in Section 7.2. Finally, the results of the quotient-based matching method are given in Section 7.3.

### 7.1. Semi-quotient matching

To evaluate the semi-quotient space matching we first converted the estimated functional map to a point-to-point map. For this we used the method described in [OBCS\*12] based on finding the nearest delta-function on the target shape to the image of a given delta-function on a source shape. Note that in this case, we have to project each delta function on the target onto the space  $L^2_+$ , and since symmetric points will have the same projection in this space, the point-to-point map can arbitrarily flip between a point and its symmetric counterpart.

We then evaluated the resulting point-to-point map  $T : M \rightarrow N$ , by computing, for every point  $x$  in the benchmark, the minimum between the distances  $d(T(x), x')$  and  $d(T(x), S(x'))$ , where  $x'$  is the ground truth correspondence for  $x$  and  $S : N \rightarrow N$  is the ground truth symmetry on  $N$ . Figure 6 shows the fraction of correspondences against the geodesic distance computed as above (See [KLF11] for the description of the scale). We also compare our method to two state-of-the-art techniques: Blended Intrinsic Maps (BIM) [KLF11] and the original functional maps method in [OBCS\*12] on the same dataset. We stress that unlike these methods, our technique does not rely on any landmark correspondences, and computes the point-to-point map only during post-processing. In particular, this allows us to achieve comparable results at only the fraction of the time. For example, on this dataset we achieve a 5x speedup compared to the functional maps technique, which uses an expensive combinatorial search to establish part correspondences.

### 7.2. Symmetry transfer

While the results for semi-quotient matching are comparable to those of other methods, they can further be improved by using them for the symmetry transfer followed by quotient-space matching described in Section 4. Thus, we first use

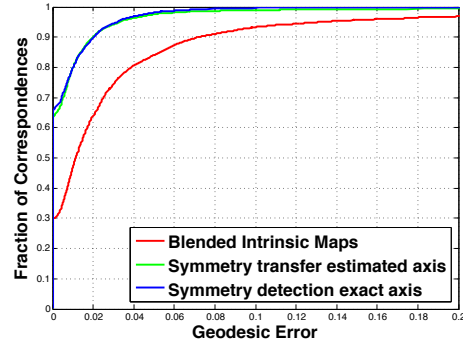


**Figure 8:** Geodesic error for symmetry detection on the TOSCA dataset, using estimated and exact symmetry axes.

these results to estimate the symmetry. Namely, we compute the distance function on the undeformed version of each shape in the dataset, and use the correspondences computed earlier, to transfer it onto the source shape. We then perform persistence-based clustering to find two clusters and use constraint splitting to estimate the symmetry on each shape. Note that this process is very robust since persistence-based clustering is very global in nature and can recover from local errors in the map. Figure 7 shows the process of symmetry estimation through transfer on one of the dog shapes. Note also that the symmetry estimation method only uses the map to the target shape to estimate the symmetry axis. Therefore, one can compare the results of this technique to the case where the symmetry axis is specified *and no target shape is used*.

We evaluated this symmetry estimation by computing the geodesic error of the computed correspondences. In this case there is no ambiguity in the result, since we assume exactly one reflectional symmetry on each shape. We also compared the maps generated by our method with Blended Intrinsic Maps-based symmetry detection. Note that BIM was introduced as a shape matching technique in [KLF11], and in [LKF12], the authors give a brief evaluation of BIM as a symmetry detection method, concluding that it gives state-of-the-art results for symmetry detection. Figure 8 gives the quantitative results obtained with the two methods on the TOSCA dataset, whereas Figure 9 illustrates some exemplar results. Note that our method shows significant improvement in the quality of the final symmetry compared to BIM which is not able to capture high-frequency features close to the symmetry axis.

### 7.3. Quotient-based shape matching

Finally, we use these results for quotient-based shape matching, as explained in Section 6.2. Figure 10 shows the results of quotient-space matching on the TOSCA dataset. To avoid clutter, we only plot the error for one of the two possible maps between each pair of shapes. Note that unlike the plot in Figure 6, in this evaluation we only allow the flipping of the entire maps, and not of every point. Thus, we consider,

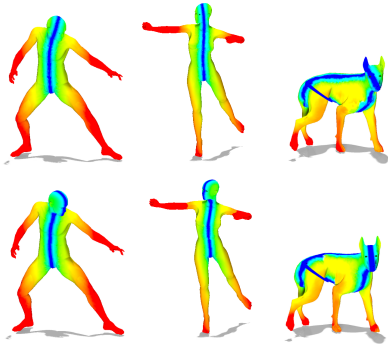


**Figure 9:** Symmetry maps obtained on the TOSCA dataset using BIM (first row), and using our method (second row): compared to BIM, the improvement achieved by our method is noticeable especially on regions close to the symmetry axis, encompassing high-frequency features.

for every map, its average error with respect to the direct and ground truth symmetry map, and then compute the per-point evaluation based on the ground truth that had the smaller error. The same procedure was used in the original BIM benchmark [KLF11] to evaluate intrinsic matching.

As can be seen in Figures 10 and 11, the quality of the final maps computed with our method is significantly better than that of both the original functional maps framework and BIM. We also compared our technique to the recently proposed method for computing correspondences using symmetry axes [LKF12]. To achieve a fair comparison, we assumed that in both cases the symmetry axis is exact and provided by the user. As shown in Figure 10, our method achieves a significant improvement in the results (average error lower by 2.5 times). We attribute this improvement to the reduction in the dimensionality of the solution space, which is achieved without sacrificing the representation quality.

Remarkably, the quality of the symmetry and correspondence maps obtained using the symmetry transfer method is very similar to the case when the symmetry axis is given (Figures 8 and 10), showing the robustness of the proposed transfer procedure.

#### 7.4. Parameter selection

Both the quotient and semi-quotient matching methods rely on several key parameters. Perhaps the most important is the number  $k$  of eigenvectors of the LB operator used in the matching. We set  $k = 30$  for all of the experiments in this paper (note that the dimension of the space  $L_+^2$  was estimated between 16 and 20 depending on the model). We also used the Wave-Kernel Signature with  $nt = 100$  and constraint splitting with  $s = 5$  intervals. Finally, in all of the experiments, we estimated the initial map using LB commutativity with descriptor preservation constraints. We then refined this initial map using the ICP procedure with 20 steps. Finally, we refined the initial map by converting the point-

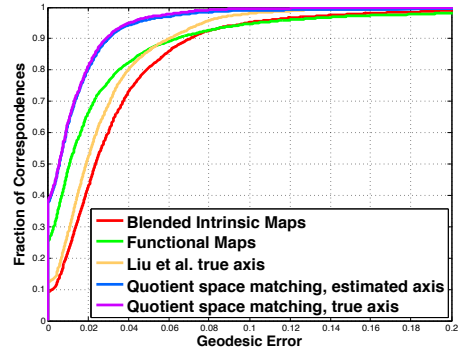


**Figure 10:** Geodesic error for shape matching on the TOSCA dataset.

to-point map and using ICP refinement with a larger number  $k$  (100 and 300) as described in Section 8.1 of [OBCS\*12].

## 8. Conclusion

In this paper, we have introduced a principled framework for performing shape matching between pairs of symmetric shapes. Our main insight is to combine the ideas of the symmetry-invariant function space [LCDF10] with the functional map framework [OBCS\*12] to show how dense correspondences can be found efficiently in this reduced space. The use of functional map framework is essential since it allows us to perform shape matching in a reduced linear space and avoid the explicit identification of symmetric points. Notably we have shown that high-quality maps can be obtained using this framework without establishing any landmark point or part correspondences, since the map between symmetric spaces is unique even in the presence of multiple isometries between the shapes.

**Limitations and future work.** While our framework is general and can, in principle, handle any pair of symmetric shapes, it still has some limitations. Most importantly, we rely on an estimation of the space  $L_+^2$ , for which we currently need at least one reference shape with a known symmetry. It would be interesting to see if this space can be estimated automatically e.g. using the method of [LCDF10]. Moreover, there is a number of key parameters, which are currently set manually. An automatic or data-driven approach would be better. Finally, our current method for extracting dense correspondences after quotient space matching only works for a limited class of symmetries (notably cyclic symmetries with a single generator), and shapes on which a fundamental domain can be consistently estimated. In the future, a more thorough investigation is necessary to extend this method to more general cases of symmetries and shapes.

**Acknowledgments.** The authors gratefully acknowledge the support of NSF grants FODAVA 808515, CCF 1161480, DMS 1228304, AFOSR grant 1156110-1-TACAD, a Google Research Award, the Max Planck Center for Visual Computing and Communications, Qualcomm/LIX postdoctoral grant, and Marie-Curie CIG grant 334283.

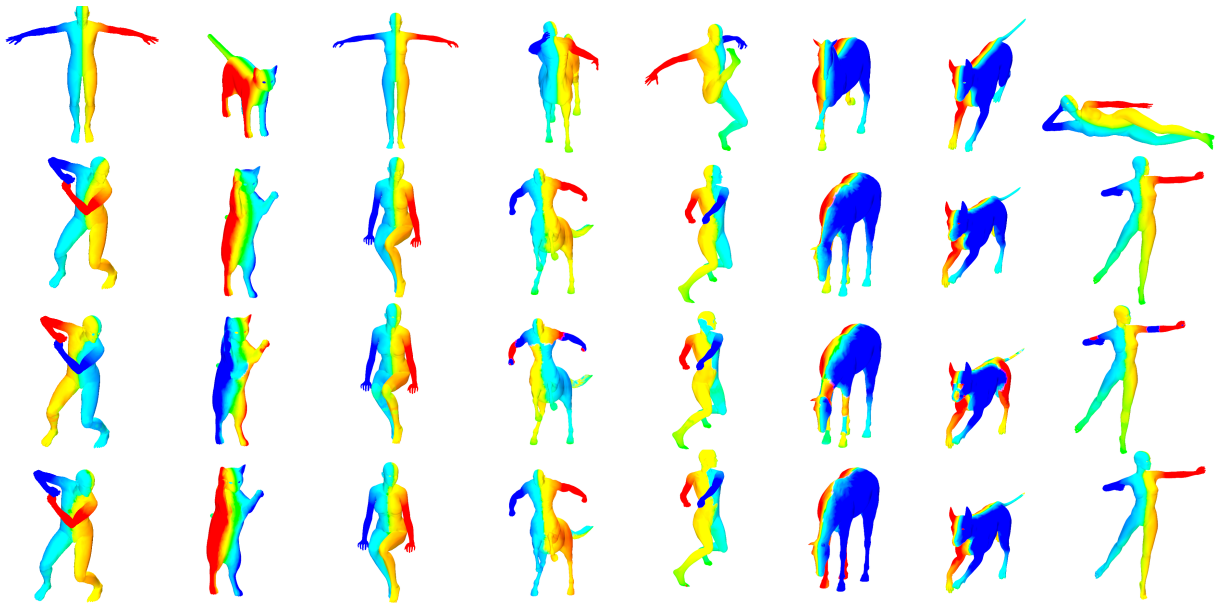


**Figure 11:** Correspondences obtained on the TOSCA dataset [BBK06] between a target shape (first row) and a source shape, using BIM [KLF11] (second row), the original functional maps approach [OBCS\*12] (third row), and our semi-quotient method (last row). Corresponding points are indicated through the same color. Note that BIM reports continuous maps, but fails in capturing the details of the shape, whereas the original functional maps method exhibits the opposite behavior. The proposed method achieves satisfactory results in terms of both, maps continuity and accuracy.

## References

- [ASC11] AUBRY M., SCHLICKEWEI U., CREMERS D.: The wave kernel signature: A quantum mechanical approach to shape analysis. In *ICCV - Workshop (4DMOD)* (2011). 3, 5
- [BBK06] BRONSTEIN A., BRONSTEIN M., KIMMEL R.: Generalized multidimensional scaling: a framework for isometry-invariant partial surface matching. *PNAS* 103, 5 (2006). 1, 11
- [BBK08] BRONSTEIN A., BRONSTEIN M., KIMMEL R.: *Numerical Geometry of Non-Rigid Shapes*. Springer, 2008. 8
- [BM77] BOYER R. S., MOORE J. S.: A fast string searching algorithm. *Commun. ACM* 20 (October 1977). 2
- [CGOS11] CHAZAL F., GUIBAS L. J., OUDOT S. Y., SKRABA P.: Persistence-based clustering in riemannian manifolds. In *Proc. SOCG* (2011), ACM, pp. 97–106. 8
- [GIRL03] GELFAND N., IKEMOTO L., RUSINKIEWICZ S., LEVOY M.: Geometrically stable sampling for the ICP algorithm. In *3DIM* (2003). 2
- [HAWG08] HUANG Q.-X., ADAMS B., WICKE M., GUIBAS L. J.: Non-rigid registration under isometric deformations. *CGF (Proc. SGP)* 27, 5 (2008), 1449–1457. 1
- [KLF11] KIM V. G., LIPMAN Y., FUNKHOUSER T.: Blended intrinsic maps. *ACM TOG (Proc. SIGGRAPH)* 30, 4 (2011). 1, 2, 8, 9, 10, 11
- [KMP77] KNUTH D. E., MORRIS J., PRATT V. R.: Fast pattern matching in strings. *SIAM Journal of Computing* 6, 2 (1977), 323–350. 2
- [LCDF10] LIPMAN Y., CHEN X., DAUBECHIES I., FUNKHOUSER T.: Symmetry factored embedding and distance. *ACM TOG (Proc. SIGGRAPH)* (2010). 2, 3, 4, 10
- [LF09] LIPMAN Y., FUNKHOUSER T.: Möbius voting for surface correspondence. In *Proc. of SIGGRAPH* (2009), vol. 28:3, pp. 72:1–72:12. 1, 2
- [LKF12] LIU T., KIM V. G., FUNKHOUSER T.: Finding surface correspondences using symmetry axis curves. In *Eurographics Symposium on Geometry Processing (SGP)* (2012). 2, 9, 10
- [OBCS\*12] OVSJANIKOV M., BEN-CHEN M., SOLOMON J., BUTSCHER A., GUIBAS L.: Functional maps: a flexible representation of maps between shapes. *ACM Trans. Graph.* 31, 4 (July 2012), 30:1–30:11. 1, 2, 3, 5, 6, 8, 9, 10, 11
- [OHG11] OVSJANIKOV M., HUANG Q.-X., GUIBAS L. J.: A condition number for non-rigid shape matching. *Comput. Graph. Forum (Proc. SGP)* 30, 5 (2011), 1503–1512. 2
- [OMMG10] OVSJANIKOV M., MERIGOT Q., MEMOLI F., GUIBAS L.: One point isometric matching with the heat kernel. *CGF* 29, 5 (2010), 1555–1564. 1, 2
- [PLC\*08] PARK M., LEE S., CHEN P.-C., KASHYAP S., BUTT A. A., LIU Y.: Performance evaluation of state-of-the-art discrete symmetry detection algorithms. In *Proc. CVPR* (2008). 2
- [RBBK10] RAVIV D., BRONSTEIN A. M., BRONSTEIN M. M., KIMMEL R.: Full and partial symmetries of non-rigid shapes. *Int. J. Comput. Vision* 89 (2010), 18–39. 2, 3
- [SOG09] SUN J., OVSJANIKOV M., GUIBAS L.: A Concise and Provably Informative Multi-Scale Signature Based on Heat Diffusion. *CGF (Proc. SGP)* 28, 5 (2009). 3
- [SY13] SAHILLIOGLU Y., YEMEZ Y.: Coarse-to-fine isometric shape correspondence by tracking symmetric flips. *Comput. Graph. Forum* 32, 1 (2013), 177–189. 1, 2
- [TBW\*09] TEVS A., BOKELOH M., WAND M., SCHILLING A., SEIDEL H.-P.: Isometric registration of ambiguous and partial data. In *Proc. CVPR* (2009), pp. 1185–1192. 1
- [TBW\*11] TEVS A., BERNER A., WAND M., IHRKE I., SEIDEL H.-P.: Intrinsic shape matching by planned landmark sampling. In *Proc. Eurographics* (2011), p. to appear. 2